JOURNAL OF MATERIALS SCIENCE 31 (1996) 5247–5256

RF magnetron sputtered aluminium oxide coatings on iridium

K. MUMTAZ, J. ECHIGOYA, H. ENOKI, T. HIRAI*, Y. SHINDO
*Department of Materials Processing, Faculty of Engineering and *Institute for Materials Research, Tohoku University, Sendai 980, Japan*

The effects of process parameters on the microstructural morphology of aluminium oxide (Al_2O_3) coatings on Ir have been studied. Al_2O_3 coatings were deposited on Ir-coated isotropic graphite (IG) substrates at substrate temperatures of room temperature (RT)–1073 K, RF power of 200–600 W in an Ar, or Ar + 1–10% O_2, sputtering gas atmosphere by RF magnetron sputtering. Al_2O_3 coatings which were deposited at high substrate temperatures and high RF powers in an Ar, or an Ar + O_2, sputtering gas atmosphere were found to contain a dense, fine columnar structure with a γ-Al_2O_3 phase, low Ar content and a relatively high hardness value of ca. 1050 H_v. Furthermore, high resolution transmission electron microscopy (HRTEM) results revealed the epitaxial growth of Al_2O_3 coatings on Ir–coated IG substrate. It was found that the interface between Al_2O_3 and Ir coatings was sharp and Al_2O_3 coatings remained intact with the Ir-coated IG substrate.

1. Introduction

Aluminium oxide (Al_2O_3) coatings have many attractive properties such as relatively low volatility, low O_2 diffusion coefficients, slow growth kinetics, excellent high temperature strength, good corrosion resistance and oxidation stability. Al_2O_3 coatings have been widely prepared by vacuum methods, i.e. physical vapour deposition (PVD) and chemical vapour deposition (CVD), because of their versatile applications in engineering. Thin Al_2O_3 coatings prepared by PVD methods are used for optical filters, microelectronics, insulating coatings on Cu electrodes and insulator modules in channels of magnetohydrodynamic generators [1, 2]. Al_2O_3 coatings are mostly deposited on metal substrates, however, Al_2O_3 coatings when deposited on carbonaceous substrates have a weak point in that they may react with C which is a strong reducing agent and may form aluminium carbide at high temperatures, which is hard and brittle [3–5].

Some Al_2O_3 coatings were sputtered directly onto isotropic graphite (IG) substrates, but this led to poor bonding of the Al_2O_3 coatings to the IG substrate. Such Al_2O_3 coatings could not be exposed to elevated temperatures without debonding from the substrate. Fig. 1 shows an example of the delamination that occurred during cooling from the high deposition temperature in run 33 (Table I).

In order to avoid decohesion and spallation, and to suppress aluminium carbide formation, an intermediate layer is necessary for high temperature applications of antioxidation Al_2O_3 coatings. Ir was selected as a barrier coating layer to provide adhesion to the graphite, to resist O_2 ingress into the carbonaceous substrate and to prevent interdiffusion of the Al_2O_3 coating and the substrate [6–8]. If Al_2O_3 coatings are intended to be used at high temperatures, one of the main requirements is good thermal stability of the as-deposited coating [9]. This includes good adherence to the Ir coating, a stable crystal structure, a low impurity level (e.g. Ar content) and a dense microstructure.

Therefore, at the outset, investigations into the growth process of Al_2O_3 coatings on Ir-coated IG substrates by the sputtering method was performed because of: (1) the successive deposition of the Al_2O_3 coating onto the Ir coating using the same vaccum chamber; and (2) the possibility to vary substrate temperature to investigate the interface structure.

In order to explore the feasibility of this approach, Al_2O_3 coatings were RF magnetron sputtered onto the Ir-coated IG substrates to study the effect of process parameters on the microstructure of Al_2O_3 coatings. Of particular interest is the effect of substrate temperature and Ar or Ar + O_2 as a sputtering gas plasma on the as-deposited Al_2O_3 coatings. This study also includes an investigation of the interface formation between Al_2O_3 and Ir coatings on IG substrates.

2. Experimental procedure

RF magnetron sputtering was used for Al_2O_3 coatings deposition on Ir-coated IG substrates. The thickness of elemental Ir on IG substrates was between 6 and 8 μm deposited at 1073 K. Details about the Ir deposition on IG have been described elsewhere [7, 8]. As for the removal of entrapped gases from the Ir-coated IG substrates prior to Al_2O_3 coating, the

0022–2461

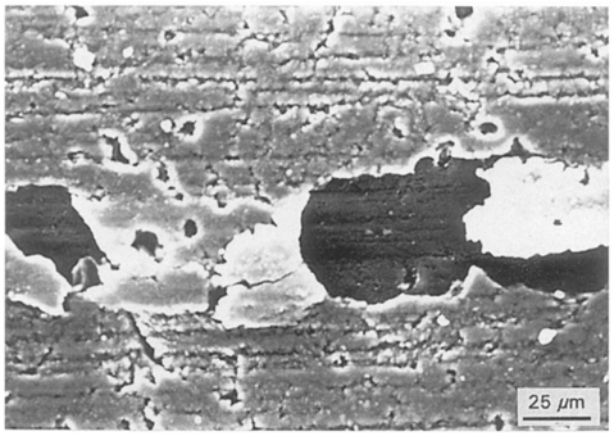

Figure 1 SEM surface view of Al_2O_3 coating on an IG substrate (run 33).

typical heating temperature was 1073 K for 54 ks (15 h) in a vacuum of 10^{-4} Pa. Prior to deposition, the Ir-coated IG substrates were sputter cleaned in a pure Ar discharge for 60 s (1 min) and the target was shielded by a rotatable shutter.

The sputtering target was a circular, high purity (99.999%) Al_2O_3 disc, 101.6 mm in diameter and 6 mm thick (supplied by ULVAC Co. Ltd). Before sputtering, the chamber was evacuated to a base pressure of $< 1.6 \times 10^{-4}$ Pa. Prior to coating deposition, the Al_2O_3 target was sputter cleaned by operating for ca. 5 min. Al_2O_3 coatings were deposited on Ir-coated IG at substrate temperatures of 323, 773 and 1073 K. Details of the process parameters and properties of RF magnetron sputtered Al_2O_3 coatings are given in Table I. Al_2O_3 coatings were deposited without breaking the vacuum over a temperature range of 773–1073 K and a RF power of 400–600 W in an Ar sputtering gas atmosphere. For room temperature (RT) deposition, substrate temperatures rose up to maximum of 387 K depending upon the RF power and sputtering time. The target–substrate spacing for Al_2O_3 coating was 50 mm.

The sputtering was carried out with either an Ar (99.999% pure) or an Ar + 1–10% O_2 sputtering gas plasma. In this study a sputtering pressure of 0.933 Pa was selected to produce Al_2O_3 coatings. After sputtering with alumina, the samples were allowed to cool down to ambient temperature *in vacuo*.

Cross-sectional fractured and plane surfaces were examined by scanning electron microscopy (SEM) (Hitachi S-530S). X-ray diffraction (XRD) patterns were obtained from the face of the specimens using a JEOL X-ray diffractometer DX-QERP 12 operated at 30 kV and 20 mA, employing a Cu target. For chemical composition analysis, energy-dispersive X-ray (EDX), X-ray photoelectron spectroscopy (XPS) and Auger electron spectroscopy (AES) were used. XPS spectra were recorded by an ESCA 750 system using MgK_α radiation (5 kV, 32 mA), with a base pressure of $< 2.7 \times 10^{-5}$ Pa. AES measurements were carried out with a JEOL JAM-7100 with a base pressure of 1.2×10^{-7} Pa; the electron beam was accelerated to 3 kV. Depth profiling was performed using a 3 kV electron beam with a beam current density of ca. 500 μA cm^{-2}, with the Ar^+ ion beam impinging at an angle of 75° with respect to the surface normal.

Transmission electron microscopy (TEM) studies were carried out with a JEOL JEM 2000 EX TEM operated at 200 kV. JEOL-3010 operated at 300 kV was used for high resolution microscopy. TEM samples were thinned by polishing with emery paper on the uncoated side. Final thinning to electron transparency was done using ion mill operated with Ar at an acceleration voltage of 5 kV. The angle between the TEM specimen surface and the ion beam was maintained at 25° until a small hole was etched into the specimen. Specimens were sputtered with C to prevent charge-up prior to SEM and TEM examinations. The Vickers indentation was used to measure the microhardness of the Al_2O_3 coatings.

3. Results and discussion

Al_2O_3 coatings have been successfully deposited on Ir-coated IG substrates at temperatures of 323–1073 K by RF magnetron sputtering. Experiments were performed using about 33 (Al_2O_3 coatings) trial runs in which Al_2O_3 coatings were sputtered using various combinations of high and low values of the process parameters. In view of the relatively large number experimental results, preference will be given to the presentation and discussion of the results revealing the effect of processing conditions on the microstructural characteristics of the as-deposited Al_2O_3 coatings. Table I summarizes the process parameters of the Al_2O_3 coatings deposited in Ar or Ar + O_2 sputtering plasma environments. The fracture cross-section SEM microstructure of Al_2O_3 coatings (run 8) is shown in Fig. 2. In the microstructure shown, two distinct coatings can be identified. The outer coating contains featureless, pore-free and dense Al_2O_3. The inner diffusion barrier coating of Ir has a columnar appearance. High substrate temperature deposited coatings of Al_2O_3 exhibit similar morphologies to those of the RT deposited Al_2O_3 coatings for any deposition parameters, the only difference being in the deposition rate. The deposition rate of Al_2O_3 coatings was lower when the substrate temperature was higher. The addition of O_2 to Ar as a sputtering gas also caused a decrease in the deposition rate [10]. The substrate heating during coating deposition had an effect on the migration and crystallization processes of the condensating coating atoms.

In this study, regardless of the deposition parameters used, an Al_2O_3 coatings deposited; although not shown here, all as-deposited Al_2O_3 coatings exhibited good adherence with Ir-coated IG substrates. Detailed examination of the fracture surface revealed that coating fracture, rather than delamination or spallation, occurred during deformation, suggesting a strong interfacial bond. The good adherence of Al_2O_3 coatings were also confirmed in cutting tests.

Cross-sectional EDX analysis to determine the Ar content in the as-deposited Al_2O_3 coatings are given in Table I. Results show low amounts of Ar present in

TABLE I Process parameters and properties of RF magnetron sputttered Al_2O_3 coatings

Coating run	RF power (W)	Substrate temperature (K)	Sputtering gas	Coating thickness of Al_2O_3 (μm)	Deposition rate of Al_2O_3 ($nm\,s^{-1}$)	Coating colour of Al_2O_3	Argon content (at. %)	Coating thickness of Ir (μm)
8	600	RT (387)	Ar	12.00	0.716	Black	1.08	6.20
10	600	1073	Ar	5.13	0.475	Brownish Black	0.25	7.32
19	600	1073	Ar + 1% O_2	4.94	0.191	Transparent	0.24	7.49
24	400	RT (315)	Ar + 5% O_2	4.80	0.11	Transparent	0.55	7.20
28	600	1073	Ar + 5% O_2	3.21	0.149	Transparent	0.20	7.34
29	600	1073	Ar + 10% O_2	3.00	0.133	Transparent	0.16	6.90
30	600	RT (312)	Ar	0.5	0.72	Coloured	–	7.20
31	600	RT (314)	Ar + 10% O_2	0.5	0.15	Coloured	–	7.00
32	600	1073	Ar + 10% O_2	0.5	0.133	Transparent	–	7.00
33	600	RT (312)	Ar + 10% O_2	1.0	0.133	Coloured	–	–

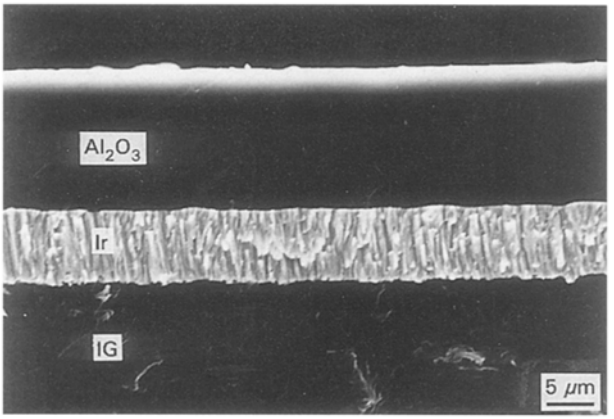

Figure 2 SEM cross-section micrograph of double layer Al_2O_3/Ir coatings on an IG substrate (run 8).

the Al_2O_3 coatings, although EDX analysis is qualitative. No other distinguishable peaks were observed in EDX analysis of the coatings, or at the coating–substrate interface, for any of the specimens examined in this study. Ar was the common impurity in all of the Al_2O_3 coatings, as observed by EDX analysis. The Ar content in the coatings varied depending on the sputtering parameters and it was found to decrease with substrate temperature. This may be due to the decrease in sticking probability of inert Ar sputter gas with increasing substrate temperature [11]. Addition of O_2 also resulted in a lower Ar content. It seems that at high O_2 contents the resputtered O_2 might become ionized by collosion with Ar^+ ions and help in increasing the stoichiometry resulting in the decrease of Ar content. The best parameters for reduced Ar content seems to be high deposition temperature (1073 K) and an Ar + O_2 sputtering gas plasma.

The chemical analysis of the Al_2O_3 coatings were performed by AES and XPS. Al_2O_3 films with thicknesses of 500 nm were prepared on Ir-coated IG substrates under the process parameters shown in Table I. AES and XPS results from a single crystal of α-Al_2O_3 were also obtained, which are considered as standard data.

AES spectra of Al_2O_3 films before Ar^+ ion etching are shown in Fig. 3. The Al (L M M) signal of Al_2O_3 occurs at 49 eV. Two more Al (K L L) signals of Al_2O_3 can be seen at 1328 and 1381 eV. The peaks at 266 and 501 eV are assigned to the signals from C and O_2, respectively. *In situ* Ar^+ ion sputter etching of an Al_2O_3 film was performed at an energy of 3 kV with a beam intensity of 500 $\mu A\,cm^2$. Sputter rates were calibrated using SiO_2 as reference. The etching rate of Al_2O_3 was ca. 5 $nm\,min^{-1}$.

Fig. 4 shows the AES spectra after 20 min of *in situ* Ar^+ ion sputter etching of Al_2O_3 films. The C signal although significantly reduced, is still visible with a peak intensity of ca. 1.5%. After *in situ* Ar^+ ion sputter etching an additional peak at 60 eV is observed; this signal is more obvious in run 32 and on an α-Al_2O_3 single crystal. Furthermore, the presence of a N peak at 374 eV in the *in situ* Ar^+ ion sputter etched samples can be seen; this peak is present even on the α-Al_2O_3 single crystal.

Auger depth profiles from the as-deposited Al_2O_3 coatings for runs 30–32 are shown in Fig. 5. Slight C contamination was detected in the Al_2O_3 coatings. It should be noted that no Ir layer is distinct and no penetration or interdiffusion of either coatings are observed even in the high deposition temperature run (run 32) (Fig. 5c). The chemical compositions of the coatings are shown in Table II: the ratio of O: Al for runs 30–32 are 1.469, 1.525 and 1.433, respectively.

XPS was used to obtain information on the binding states of the Al_2O_3 coatings. The differences in binding energy (ΔE_b) was used to estimate the chemical bonding states in Al_2O_3 coatings because of the electric charge-up of the samples. E_b for O (1s) and Al (2s), and their ΔE_bs are shown in Table III. All samples show the bonding state of Al_2O_3 coatings (independent of the crystal structure of as-deposited Al_2O_3 coatings, i.e. amorphous or γ-Al_2O_3 phase) are close to that of single crystal α-Al_2O_3. No signal, for N was detected by XPS analysis.

The results of AES and XPS analyses show that Ar implanted during sputtering can be reduced by a high substrate temperature and an addition of O_2 to the Ar sputtering gas plasma. C was the main contamination, as observed by AES. The carbonaceous substrate and ambient atmosphere may be the source of contamination. Fig. 5b shows the Al_2O_3 coatings which were deposited at RT with addition of O_2 as a sputtering gas plasma resulted in the reduction of the C content.

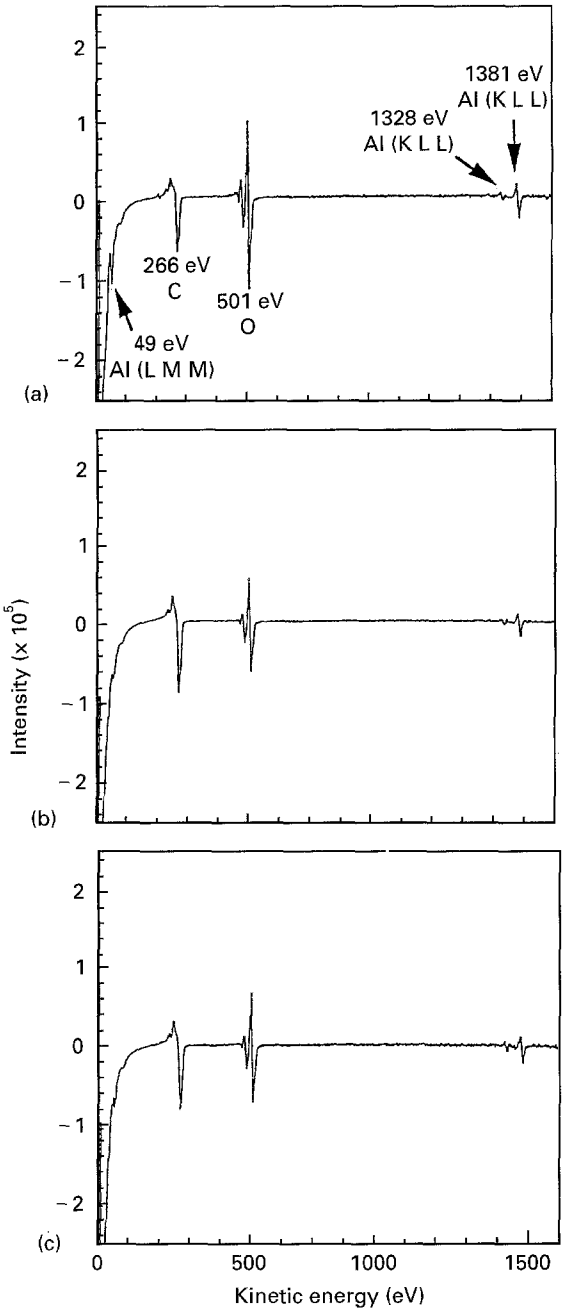

Figure 3 AES spectra of Al_2O_3 films before Ar^+ ion sputter etching: (a) run 30; (b) run 31; (c) run 32.

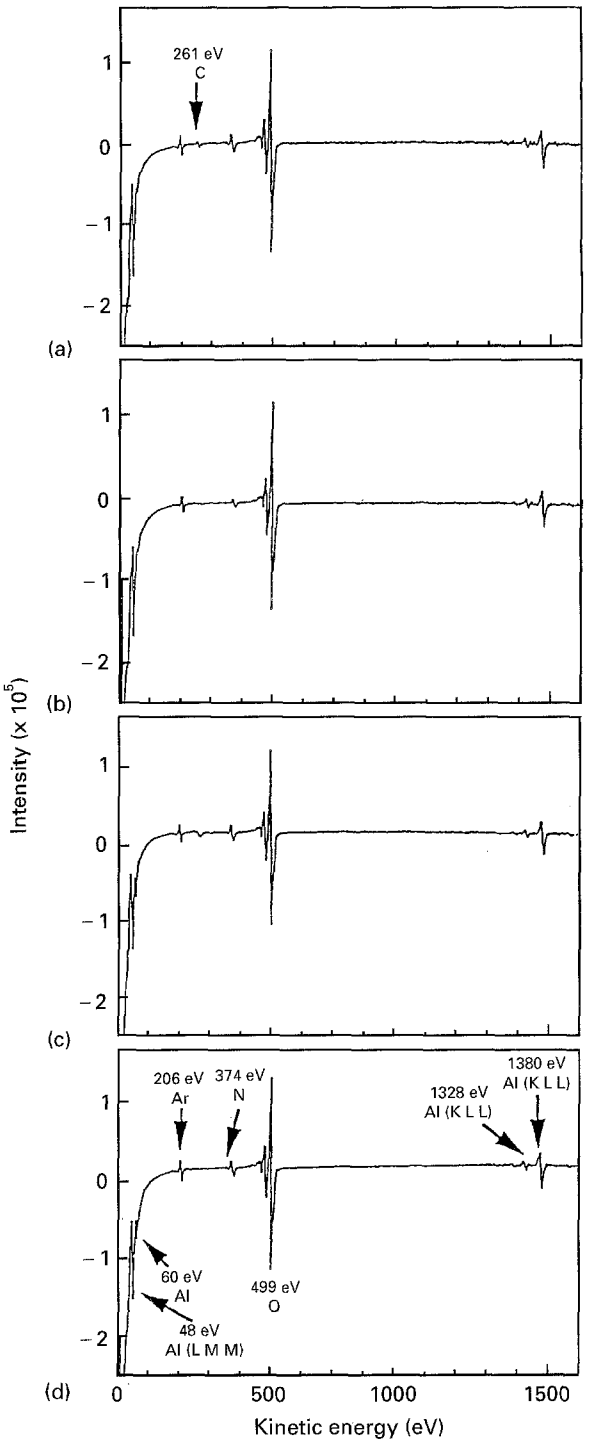

Figure 4 AES spectra of Al_2O_3 films after 20 min *in situ* Ar^+ ion sputter etching: (a) run 30; (b) run 31; (c) run 32; (d) single crystal α-Al_2O_3.

On the other hand, Al_2O_3 coatings deposited at high substrate temperatures contain relatively high amounts of C (Fig. 5c). It seems that at high temperatures, deposition C was emitted from the graphite substrate, the walls of sputtering chamber and from the heater.

The presence of the N peak at 374 eV shown by AES analysis may be due to the presence of contaminates in the AES gas inlet because XPS analysis detected no N signal.

AES and XPS analyses revealed that the (C + O): Al ratio was ca. 1.5, as shown in Fig. 5, in the present experiments within experimental error of $\pm$ 0.06. A slight decrease in the O_2 content and the C contamination in some samples reduced the apparent stoichiometry.

Al_2O_3 coatings which were deposited at 773–1073 K substrate temperatures and 400–600 W RF power in an Ar sputtering gas atmosphere, and breaking the vacuum, resulted in milky white paste-like coatings. These coatings were loosely adherent to the Ir-coated IG substrates. In order to avoid this, Al_2O_3 coatings were deposited using the same parameters but without breaking the vacuum, i.e. Al_2O_3 coatings were deposited after Ir deposition using the same vacuum. This paste-like coating effect was not observed in the case of Ar + O_2 sputtering gas plasma. The same results were also observed by Nowicki [12] after 24 h steam autoclave treatment of an Al_2O_3 coating at 120 °C and 2.03×10^5 Pa pressure. He also reported the loosely adherent, frosted microstructure of Al_2O_3 and

suggested the formation of AlO(OH) by the hydrolysis of Al. Due to the venting of the chamber to air and loading of the specimens in the chamber, slight amounts of H_2O vapour may have contaminated the walls of the chamber. It seems that the O_2, air or H_2O vapour present in the vacuum chamber during sputtering may result in the formation of AlO(OH), which can significantly alter the structure and deposition rate of the Al_2O_3 coatings. Therefore, the presence of H_2O vapour and O_2 species in the vacuum system affected the coating qualities and deposition rate.

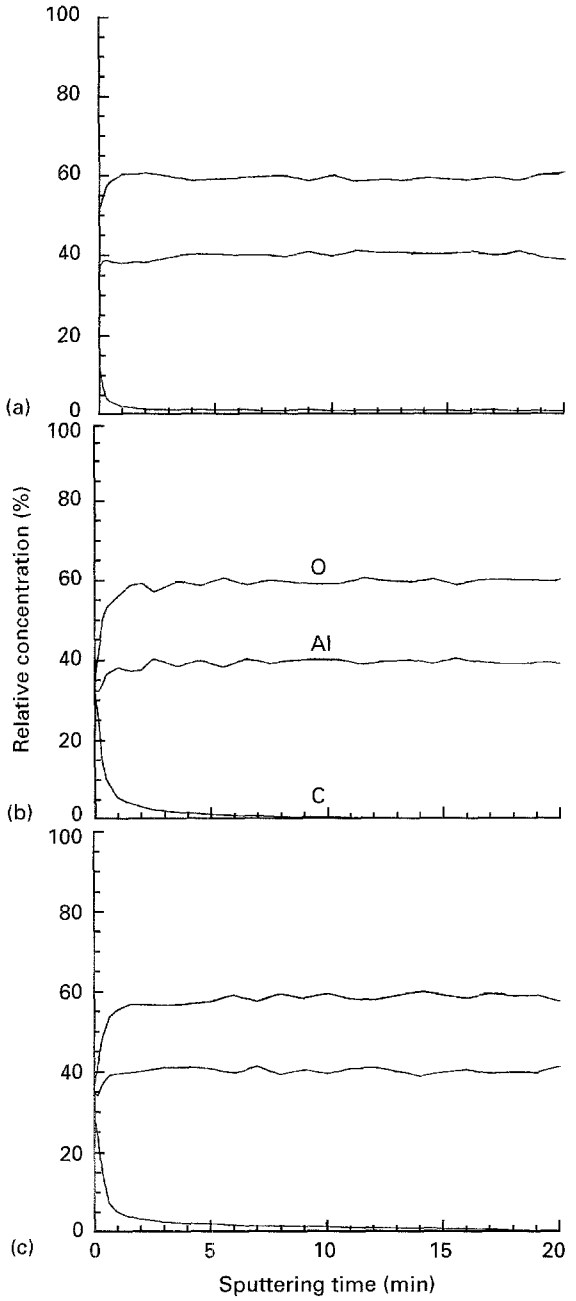

Figure 5 AES depth profile of the Al_2O_3 films: (a) run 30; (b) run 31; (c) run 32.

The typical SEM microstructure of ca. 3 (run 29)–12 μm (run 8) thick Al_2O_3 coatings shows dense, smooth and homogeneous coatings (Fig. 6a and b). The surface morphologies of Al_2O_3 coatings which were deposited using Ar only are almost the same as those deposited with an $Ar + O_2$ sputtering gas plasma. No signs of microcracking were observed and coatings remained adherent to the Ir-coated IG substrate. Although the coefficients of thermal expansion (CTE) of Al_2O_3, Ir and IG are different, the microstructure clearly shows no cracking in the coatings (CTE: $Al_2O_3 = 9.4 \times 10^{-6}\ K^{-1}$; $Ir = 8.2 \times 10^{-6}\ K^{-1}$; $IG = 7.6 \times 10^{-6}\ K^{-1}$; all at 1073 K). It had also been verified by reheating the Al_2O_3 coatings (runs 8 and 29) for 345.6 ks (96 h) at 1073 K in a vacuum chamber.

Thermal residual stresses are developed in the coatings during cooling from high deposition temperatures. Generally, tensile stresses are known to produce cracking and can influence the debonding of the coatings. It seems that the sputtered Al_2O_3 coatings on Ir-coated IG substrates were compressively stressed after cooling from high deposition temperatures, which may have inhibited the microcracking in the double-layer coatings system.

The microstructure of the coatings varied with substrate temperature, RF power and sputtering gas mixture. Fig. 7a shows a TEM micrograph of Al_2O_3 coatings (run 8) and Fig. 7b the corresponding electron diffraction pattern. Fig. 7b shows a diffuse diffraction pattern indicating that the Al_2O_3 coating was amorphous, as would be expected for this deposition temperature. The Al_2O_3 coatings which were either deposited at a RF power of 200–400 W and a low substrate temperature, i.e. RT, in Ar or Ar + 1–5% O_2 sputtering gas atmosphere were also composed of an amorphous Al_2O_3 phase. Fig. 8 shows electron diffraction pattern of an Al_2O_3 coating (run 24).

Fig. 9a shows a TEM micrograph of an Al_2O_3 coating (run 29), and Fig. 9b and c the corresponding dark field image and diffraction pattern, respectively. Fig. 9b clearly shows the average grain size of ca. 50 nm was formed in the Al_2O_3 coatings. When

TABLE II Chemical composition of Al_2O_3 films by AES

No.	Run 30		Run 31		Run 32	
	Al (at. %)	O (at. %)	Al (at. %)	O (at. %)	Al (at. %)	O (at. %)
1	39.7	60.3	39.9	60.1	40.4	59.6
2	40.2	59.8	39.5	60.5	41.1	58.9
3	40.6	59.4	39.3	60.7	41.7	58.3
4	40.8	59.2	40.0	60.0	40.6	59.4
5	41.2	58.8	39.1	60.9	41.9	58.1
Av.	40.5	59.5	39.6	60.4	41.1	58.9
SD	0.5	0.5	0.4	0.4	0.6	0.6
Al:O	1:1.469		1:1.525		1:1.433	

TABLE III Binding energy, E_b, of O(1s), Al(2s) and their difference ΔE_b

Coating run	E_bO(1s) (eV)	E_bAl(2s) (eV)	$\Delta E_b = E_b$O(1s) − Al(2s) (eV)
30	533.25	121.05	412.20
31	533.00	120.70	412.30
32	533.10	120.80	412.30
α-Al_2O_3	533.15	120.95	412.20

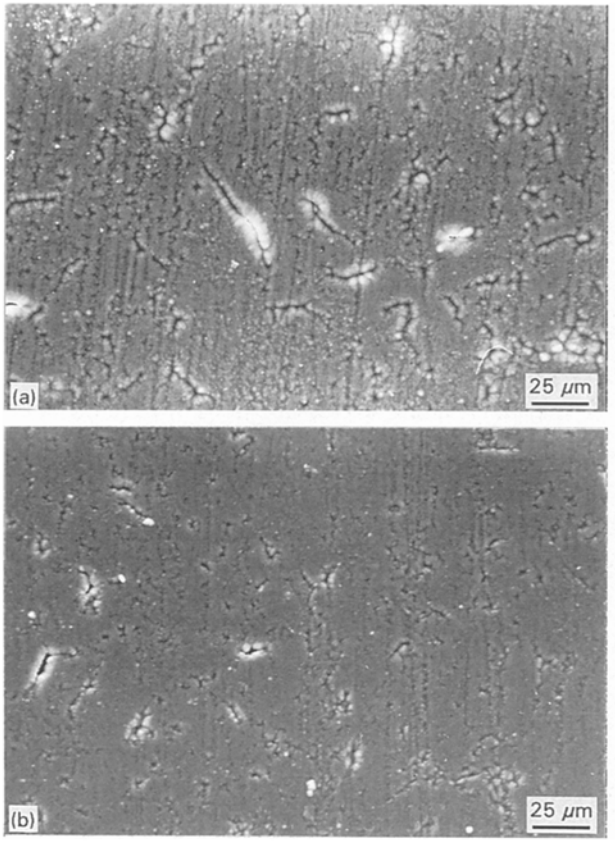

Figure 6 SEM surface views of Al_2O_3 coatings on Ir-coated IG substrates: (a) run 8, (b) run 29.

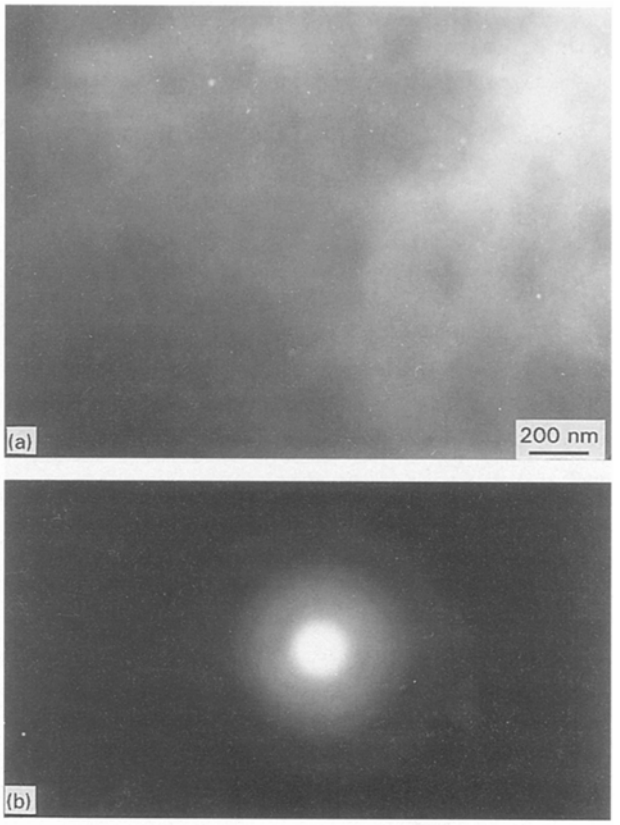

Figure 7 TEM micrographs of Al_2O_3 coatings (run 8): (a) bright field; (b) electron diffraction pattern.

Ar + 10% O_2 was used as a sputtering gas, the crystalline γ-Al_2O_3 grains became larger in size. It seems that a low deposition rate and a high substrate temperature induced grain growth. Furthermore, the transition of the Al_2O_3 coatings from an amorphous to crystalline structure was associated with an increase in the surface diffusion of adatoms by using high substrate temperatures and Ar + O_2 as a sputtering gas. Although not shown here, fine grains of ca. 20–30 nm were formed in the Al_2O_3 coatings (runs 19 and 28). Fine-dotted diffraction ring patterns were observed which showed that the crystalline γ-Al_2O_3 phase was formed in those coatings.

Fig. 9c clearly shows a diffraction ring pattern of γ-Al_2O_3, diffraction from no other phase or compound was observed. For coatings deposited at a substrate temperature of 773 K and a RF power of 600 W, in Ar or an Ar + 1–5% O_2 sputtering gas, very fine γ-Al_2O_3 crystallites were nucleated in the coatings. Fig. 10a shows TEM cross-sectional micrograph of Al_2O_3 coatings on Ir-coated IG substrates (run 29); Fig. 10b is the corresponding electron diffraction pattern. The electron diffraction pattern in Fig. 10b was obtained from a region containing Al_2O_3 and Ir coatings while excluding the IG substrate. Fig. 10a shows that a dense, fine columnar structure was formed in the Al_2O_3 coatings. It also shows no porosity

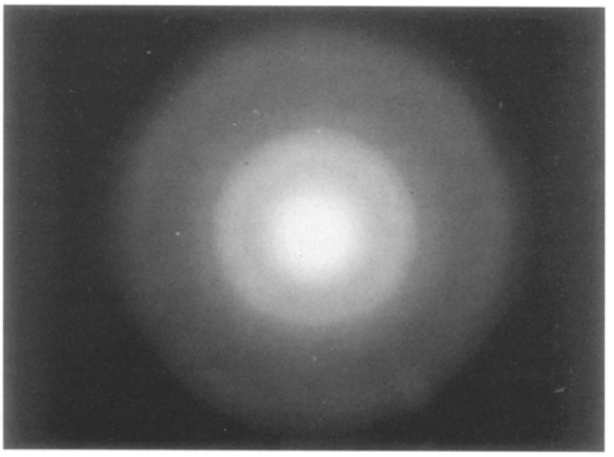

Figure 8 Electron diffraction pattern of Al_2O_3 coatings (run 24).

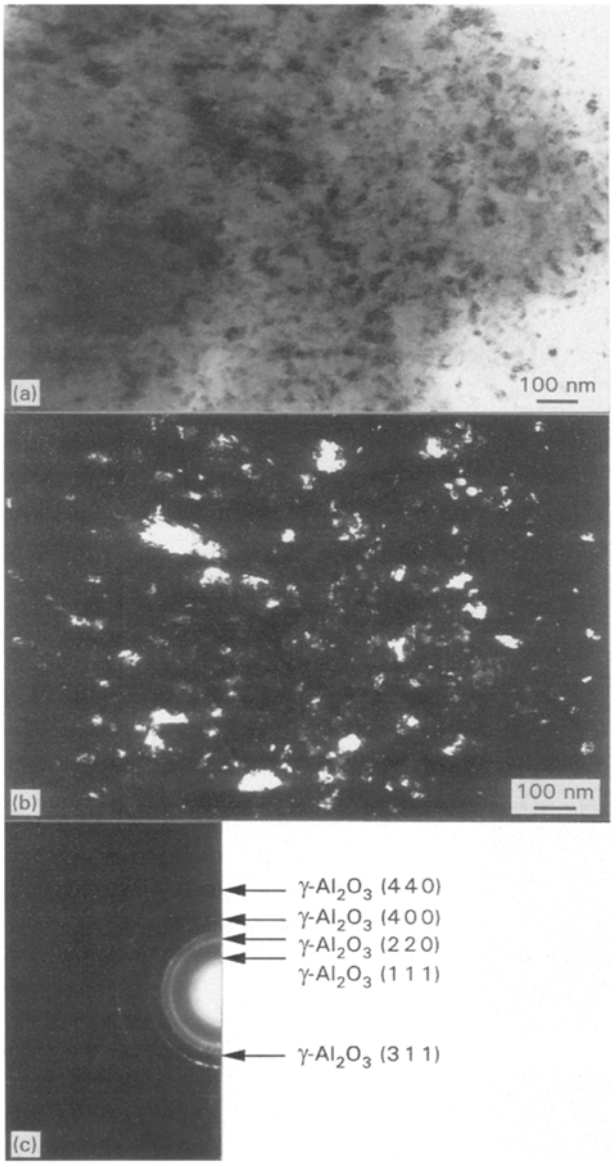

Figure 9 TEM micrographs of Al_2O_3 coatings (run 29): (a) bright field; (b) dark field; (c) electron diffraction pattern.

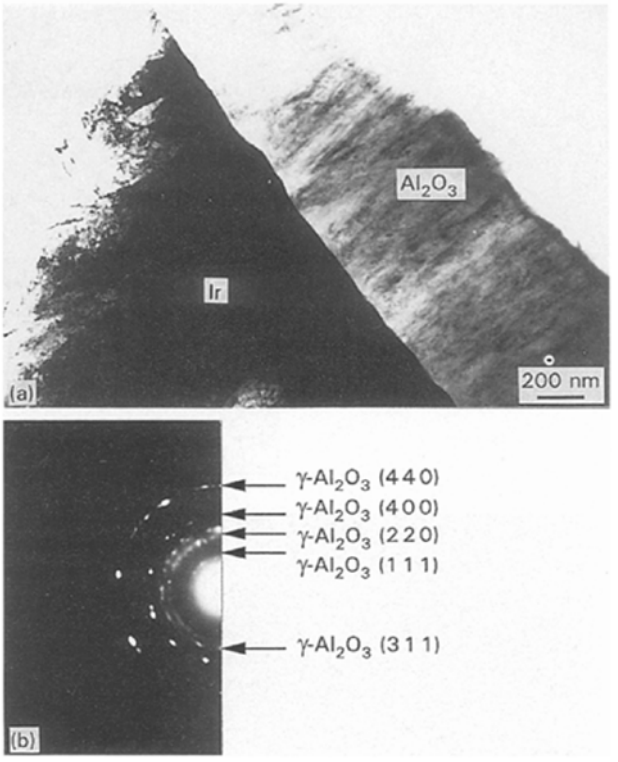

Figure 10 TEM cross-section micrographs of double layer Al_2O_3/Ir on an IG substrate (run 29): (a) bright field, (b) electron diffraction pattern.

in the coating. The electron diffraction pattern of these grains (Fig. 10b) indexing the pattern shows that only γ-Al_2O_3 was present.

The interface in Fig. 10a is sharp even though the Al_2O_3 coatings were deposited at a high substrate temperature, high RF power and Ar + up to 10% O_2 as a sputtering gas. EDX results are in agreement with the result obtained by plane and cross-sectional TEM of the same specimens. By using an Ir barrier, the reaction between C and Al was not observed up to substrate temperatures of 1073 K even though as-deposited Al_2O_3 coatings contain surface pits, as shown in Fig. 6a and b.

Fig. 11a–c shows typical HRTEM micrographs and selected-area electron diffraction (SAED) pattern from as-deposited Al_2O_3/Ir coatings on an IG substrate (run 29). Fig. 11a shows an HRTEM micrograph obtained from an Al_2O_3/Ir interface, with the electron beam parallel to the [1 1 0] Ir. The diffraction pattern analysis in Fig. 11b shows that there was usually an orientation relationship between the γ-Al_2O_3 and Ir of the form (1 1 1) Al_2O_3/(1 1 1) Ir. The SAED pattern consists of two sets of diffraction spots, representing a cubic structure ($a_0 = 0.789$ nm) corresponding to γ-Al_2O_3 together with "twins", as shown in Fig. 11b. The SAED pattern in Fig. 11c shows diffraction from Ir.

A crystalline γ-Al_2O_3 phase was identified in the top Al_2O_3 coating. The γ-Al_2O_3 phase can be seen to grow directly on the top of the Ir coating. The micrograph indicates that there is a direct correspondence between the edges of Ir crystallites and the γ-Al_2O_3 and Ir (1 1 1) surface succeed to γ-Al_2O_3 (1 1 1). Fig. 11a also shows epitaxy between the (1 1 1) in γ-Al_2O_3 and the (1 1 1) planes in the Ir: Al_2O_3 is almost parallel to the interface in this instance. The (1 1 1) planes of atoms in the Ir coating continue into the Al_2O_3 coating with d (Al_2O_3) = 0.456 nm and d (Ir) = 0.2217 nm, and also direct stable growth on the Ir coating. The misfit strain between Ir and γ-Al_2O_3 phases with the orientation relationship of $(h\,k\,l)/(h\,k\,l)$ was ca. 2.69%, which is very small and this is the reason for $(h\,k\,l)/(h\,k\,l)$ growth of γ-Al_2O_3. HRTEM Fig. 11a, revealed the formation of "twins" with a (1 1 1) twinning plane in the γ-Al_2O_3 coating. Furthermore, it also reveals a pattern which consists of two zone diffractions with an angle of 70°, which also may be viewed as a single pattern of an area with two different {1 1 1} twinning planes. This information suggests that in the crystalline Al_2O_3 phase, "twins" may had developed during deposition through the layer displacement. It may also have undergone growth when using these process parameters.

The effect of indentation on the as-deposited Al_2O_3 coatings on Ir-coated IG substrates was examined. Fig. 12a and b shows SEM micrographs of indented

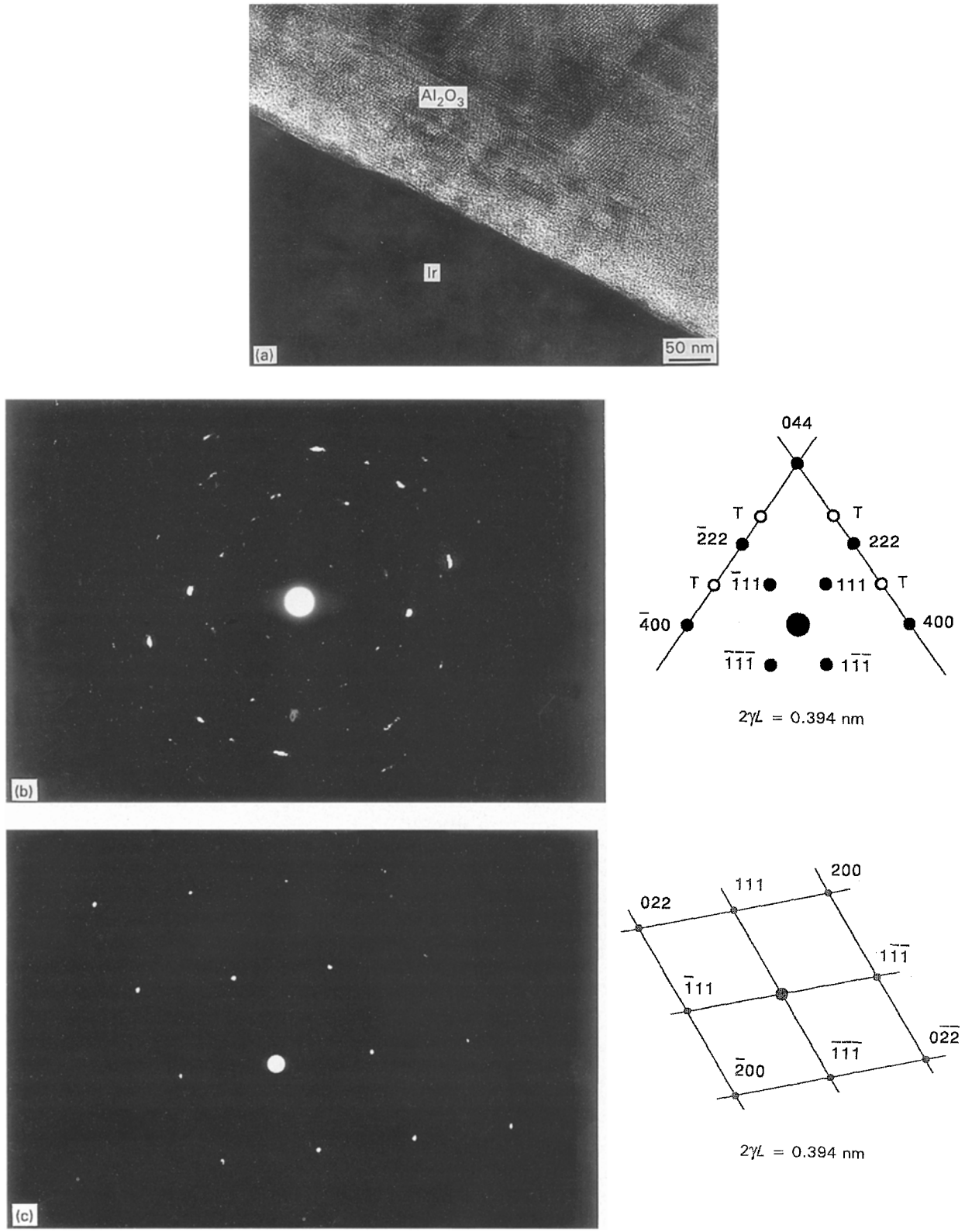

Figure 11 High-resolution TEM micrograph and SAED patterns of Al_2O_3/Ir coatings (run 29). (a) HRTEM micrograph of interface (top half is Al_2O_3 and the bottom half is Ir); (b) SAED pattern from Al_2O_3 coating, (c) SAED pattern from Ir coating.

Al_2O_3 coatings (runs 8 and 29). The indentations were produced with a 2.94 N load normal to the Al_2O_3 coating. Fig. 12c shows an SEM micrograph of an Al_2O_3 coating (run 8) indented with a load of 4.9 N. At each load, 15–20 indentations were made and the results averaged. The coating thickness for runs 8 and 29 were ca. 12 and 3 μm, respectively. Fig. 13 shows microhardness as a function of indentation load on Al_2O_3 coatings (runs 8 and 29). The analysis of the indentations showed that (run 8) cracks did not form in the load range 0.98–3.92 N, where hardness decreased from 860 to $844H_v$. However, cracks were formed for loads > 4.9 N, and their length increased with increasing load, where the hardness value was ca. $830H_v$. On the other hand, (run 29), hardness values decreased from 1053 to $1042H_v$ as the load increased from 0.98 to 3.92 N with no crack formation in the coatings. At a load of 2.94 N, the average hardness

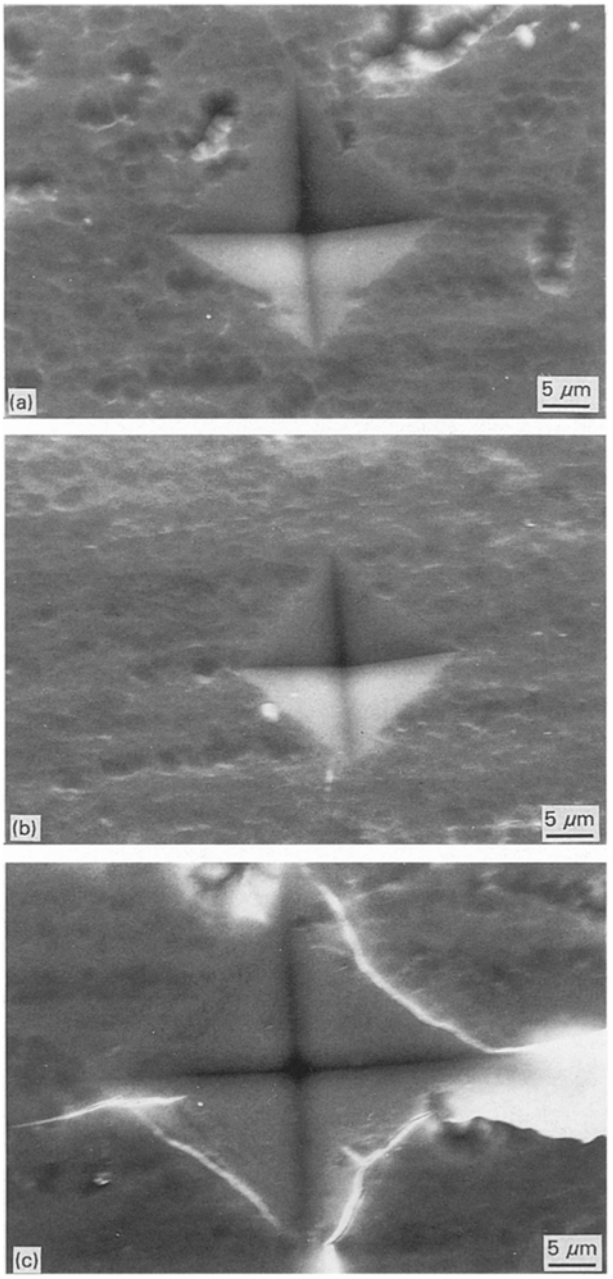

Figure 12 SEM micrographs of indented Al_2O_3 coatings; (a) run 8, load 2.94 N; (b) run 29, load 2.94 N, (c) run 8, load 4.9 N.

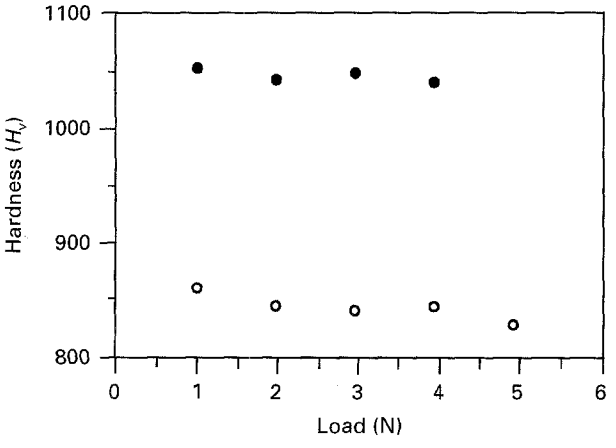

Figure 13 Vickers hardness (H_v) as a function of indentation load (N) for Al_2O_3 coatings: (○) Run 8; (●) run 29.

values were ca. 840 (run 8) and $1050H_v$ (run 29) for indentation depths >1 μm. These hardness values indicate the hardness of amorphous and γ-Al_2O_3 because the hardness of Ir coatings was $480H_v$ [7], which is smaller than those of amorphous and γ-Al_2O_3 coatings. These hardness values are smaller than that of bulk polycrystalline α-Al_2O_3, which is ca. $2000H_v$ (ca. 20 GPa) [13]. This indicates that the coating is composed of amorphous or metastable γ-Al_2O_3, which are both softer than α-Al_2O_3. SEM micrographs (Fig. 12a and b) clearly show that coated Al_2O_3 layers are not cracked and no flaking of the coatings was observed. On the other hand, Fig. 12c shows that some faint cracks were formed at the corners of impressions made at a 4.9 N load.

4. Conclusions

The conclusions are as follows.

1. Alumina coatings which were deposited at a high substrate temperature (1073 K) and in an Ar or an Ar + O_2 sputtering gas atmosphere, resulted in dense crystalline γ-Al_2O_3 coatings with a fine columnar structure. The grain sizes in Al_2O_3 coatings were increased by increasing the percentage of O_2 in the sputtering gas mixture and substrate temperature.
2. All as-deposited thick and thin Al_2O_3 coatings exhibited good adherence with the Ir-coated IG substrates and no microcracking occurred.
3. Ar was detected in the Al_2O_3 coatings by XPS and EDS analyses. It was found to decrease with increases in substrate temperature and the percentage of O_2 in the sputtering gas mixture.
4. C contamination was observed by AES when Al_2O_3 coatings were deposited at high substrate temperatures.
5. γ-Al_2O_3 grew epitaxially on Ir with the orientation relationship of $\{hkl\}_{\gamma\text{-}Al_2O_3}/\{hkl\}_{Ir}$. γ-$Al_2O_3$ coatings contain faults such as "twins" and dislocations with high densities.
6. Hardness values of 840 H_v for amorphous Al_2O_3 coatings and 1050 H_v for crystalline γ-Al_2O_3 coatings were obtained.

Acknowledgement

The authors would like to thank Professors K. Sugimoto and N. Hara, and Dr N. Akao for their help in the AES and XPS analysis.

References

1. T. A. MANTYLA, P. J. M. VUORISTO, A. K. TELAMA and P. O. KETTUNEN, *Thin Solid Films* **126** (1985) 431.
2. P. VUORISTO, J. WAHLRROS, T. MANTYLA and P. KETTUNEN, *ibid.* **166** (1988) 255.
3. M. GUPTA, I. A. IBRAHIM, F. A. MOHAMMED and E. J. LAVERNIA, *J. Mater. Sci.* **26** (1991) 6673.
4. G. J. C. CARPENTER and S. H. J. LO, *ibid.* **27** (1992) 1827.
5. A. P. DIWANJI and I. W. HALL, *ibid.* **27** (1992) 2093.
6. J. R. STRIFE and J. E. SHEEHAN, *Ceram. Bull.* **67** (1988) 369.
7. K. MUMTAZ, J. ECHIGOYA, T. HIRAI and Y. SHINDO, *Mater. Sci. Eng.* **A167** (1993) 187.

8. K. MUMTAZ, J. ECHIGOYA, H. ENOKI, T. HIRAI and Y. SHINDO, *J. Mater. Sci.* in press.
9. P. VUORISTO, T. MANTYLA and P. KETTUNEN, *Thin Solid Films* **204** (1991) 297.
10. G.-L. CHEN, J. M. SIVERTSEN and J. H. JUDY, *Mater. Lett.* **5** (1984) 196.
11. P. VUORISTO, T. MANTYLA and P. KETTUNEN, *J. Mater. Sci.* **27** (1992) 4985.
12. R. S. NOWICKI, *J. Vacuum Sci. Technol.* **14** (1977) 127.
13. G. V. SAMSONOV, "The Oxide Handbook" (IFI–Plenum, New York, 1973) p. 256.

Received 14 September 1994
and accepted 13 February 1996